Direct core structuring of microstructured optical fibers using focused ion beam milling

Stephen C. Warren-Smith,[1,*] Ricardo M. André,[1,2] Christopher Perrella,[3] Jan Dellith,[1] and Hartmut Bartelt[1]

[1]*Leibniz Institute of Photonic Technology (IPHT Jena), Albert-Einstein-Straße 9, 07745 Jena, Germany*
[2]*INESC Porto and Department of Physics and Astronomy, Faculty of Sciences, University of Porto, Rua do Campo Alegre 687, 4150-179 Porto, Portugal*
[3]*Institute for Photonics and Advanced Sensing (IPAS) and School of Physical Sciences, The University of Adelaide, Adelaide 5005, Australia*
[*]*stephen.warrensmith@ipht-jena.de*

Abstract: We demonstrate the use of focused ion beam milling to machine optical structures directly into the core of microstructured optical fibers. The particular fiber used was exposed-core microstructured optical fiber, which allowed direct access to the optically guiding core. Two different designs of Fabry-Perot cavity were fabricated and optically characterized. The first cavity was formed by completely removing a section of the fiber core, while the second cavity consisted of a shallow slot milled into the core, leaving the majority of the core intact. This work highlights the possibility of machining complex optical devices directly onto the core of microstructured optical fibers using focused ion beam milling for applications including environmental, chemical, and biological sensing.

OCIS codes: (050.2230) Fabry-Perot; (060.2370) Fiber optics sensors; (060.4005) Microstructured fibers; (230.4000) Microstructure fabrication.

References and links

1. P. Kaiser and H. W. Astle, "Low-loss single-material fibers made from pure fused silica," Bell Syst. Tech. J. **53**(6), 1021–1039 (1974).
2. P. Russell, "Photonic crystal fibers," Science **299**(5605), 358–362 (2003).
3. J. C. Knight, T. A. Birks, P. S. J. Russell, and D. M. Atkin, "All-silica single-mode optical fiber with photonic crystal cladding," Opt. Lett. **21**(19), 1547–1549 (1996).
4. T. A. Birks, J. C. Knight, and P. S. J. Russell, "Endlessly single-mode photonic crystal fiber," Opt. Lett. **22**(13), 961–963 (1997).
5. R. F. Cregan, B. J. Mangan, J. C. Knight, T. A. Birks, P. S. J. Russell, P. J. Roberts, and D. C. Allan, "Single-mode photonic band gap guidance of light in air," Science **285**(5433), 1537–1539 (1999).
6. S. Afshar V, W. Q. Zhang, H. Ebendorff-Heidepriem, and T. M. Monro, "Small core optical waveguides are more nonlinear than expected: experimental confirmation," Opt. Lett. **34**(22), 3577–3579 (2009).
7. J. M. Dudley, G. Genty, and S. Coen, "Supercontinuum generation in photonic crystal fiber," Rev. Mod. Phys. **78**(4), 1135–1184 (2006).
8. J. K. Ranka, R. S. Windeler, and A. J. Stentz, "Visible continuum generation in air-silica microstructure optical fibers with anomalous dispersion at 800 nm," Opt. Lett. **25**(1), 25–27 (2000).
9. W. J. Wadsworth, R. M. Percival, G. Bouwmans, J. C. Knight, T. A. Birks, T. D. Hedley, and P. S. J. Russell, "Very high numerical aperture fibers," IEEE Photonic. Tech. L. **16**, 843–845 (2004).
10. K. Furusawa, A. Malinowski, J. Price, T. Monro, J. Sahu, J. Nilsson, and D. Richardson, "Cladding pumped ytterbium-doped fiber laser with holey inner and outer cladding," Opt. Express **9**(13), 714–720 (2001).
11. J. K. Sahu, C. C. Renaud, K. Furusawa, R. Selvas, J. A. Alvarez-Chavez, D. J. Richardson, and J. Nilsson, "Jacketed air-clad cladding pumped ytterbium-doped fibre laser with wide tuning range," Electron. Lett. **37**(18), 1116–1117 (2001).
12. T. M. Monro, S. Warren-Smith, E. P. Schartner, A. Francois, S. Heng, H. Ebendorff-Heidepriem, and S. Afshar, "Sensing with suspended-core optical fibers," Opt. Fiber Technol. **16**(6), 343–356 (2010).
13. T. M. Monro, W. Belardi, K. Furusawa, J. C. Baggett, N. G. R. Broderick, and D. J. Richardson, "Sensing with microstructured optical fibres," Meas. Sci. Technol. **12**(7), 854–858 (2001).
14. S. Silva, P. Roriz, and O. Frazao, "Refractive index measurements of liquids based on microstructured optical fibers," Photonics **1**(4), 516–529 (2014).

#250288 Received 16 Sep 2015; revised 15 Dec 2015; accepted 21 Dec 2015; published 7 Jan 2016

15. Y. Zhu, H. Du, and R. Bise, "Design of solid-core microstructured optical fiber with steering-wheel air cladding for optimal evanescent-field sensing," Opt. Express **14**(8), 3541–3546 (2006).
16. S. Afshar 5th, S. C. Warren-Smith, and T. M. Monro, "Enhancement of fluorescence-based sensing using microstructured optical fibres," Opt. Express **15**(26), 17891–17901 (2007).
17. F. M. Cox, A. Argyros, and M. C. J. Large, "Liquid-filled hollow core microstructured polymer optical fiber," Opt. Express **14**(9), 4135–4140 (2006).
18. J. M. Fini, "Microstructure fibres for optical sensing in gases and liquids," Meas. Sci. Technol. **15**(6), 1120–1128 (2004).
19. G. Tsiminis, F. Chu, S. C. Warren-Smith, N. A. Spooner, and T. M. Monro, "Identification and quantification of explosives in nanolitre solution volumes by Raman spectroscopy in suspended core optical fibers," Sensors (Basel) **13**(10), 13163–13177 (2013).
20. S. C. Warren-Smith, S. Heng, H. Ebendorff-Heidepriem, A. D. Abell, and T. M. Monro, "Fluorescence-based aluminum ion sensing using a surface-functionalized microstructured optical fiber," Langmuir **27**(9), 5680–5685 (2011).
21. S. Heng, A. M. Mak, D. B. Stubing, T. M. Monro, and A. D. Abell, "Dual sensor for Cd(II) and Ca(II): selective nanoliter-scale sensing of metal ions," Anal. Chem. **86**(7), 3268–3272 (2014).
22. J. B. Jensen, L. H. Pedersen, P. E. Hoiby, L. B. Nielsen, T. P. Hansen, J. R. Folkenberg, J. Riishede, D. Noordegraaf, K. Nielsen, A. Carlsen, and A. Bjarklev, "Photonic crystal fiber based evanescent-wave sensor for detection of biomolecules in aqueous solutions," Opt. Lett. **29**(17), 1974–1976 (2004).
23. J. Jensen, P. Hoiby, G. Emiliyanov, O. Bang, L. Pedersen, and A. Bjarklev, "Selective detection of antibodies in microstructured polymer optical fibers," Opt. Express **13**(15), 5883–5889 (2005).
24. Y. Ruan, T. C. Foo, S. Warren-Smith, P. Hoffmann, R. C. Moore, H. Ebendorff-Heidepriem, and T. M. Monro, "Antibody immobilization within glass microstructured fibers: a route to sensitive and selective biosensors," Opt. Express **16**(22), 18514–18523 (2008).
25. L. V. Nguyen, K. Hill, S. C. Warren-Smith, and T. M. Monro, "Interferometric-type optical biosensor based on exposed-core microstructured optical fiber," Sensor. Actuat. Biol. Chem. **211**, 320–327 (2015).
26. D. K. C. Wu, B. T. Kuhlmey, and B. J. Eggleton, "Ultrasensitive photonic crystal fiber refractive index sensor," Opt. Lett. **34**(3), 322–324 (2009).
27. M. Hautakorpi, M. Mattinen, and H. Ludvigsen, "Surface-plasmon-resonance sensor based on three-hole microstructured optical fiber," Opt. Express **16**(12), 8427–8432 (2008).
28. A. Wang, A. Docherty, B. T. Kuhlmey, F. M. Cox, and M. C. J. Large, "Side-hole fiber sensor based on surface plasmon resonance," Opt. Lett. **34**(24), 3890–3892 (2009).
29. A. Hassani and M. Skorobogatiy, "Design of the microstructured optical fiber-based surface plasmon resonance sensors with enhanced microfluidics," Opt. Express **14**(24), 11616–11621 (2006).
30. B. Gauvreau, A. Hassani, M. Fassi Fehri, A. Kabashin, and M. A. Skorobogatiy, "Photonic bandgap fiber-based Surface Plasmon Resonance sensors," Opt. Express **15**(18), 11413–11426 (2007).
31. M. C. Phan Huy, G. Laffont, V. Dewynter, P. Ferdinand, P. Roy, J.-L. Auguste, D. Pagnoux, W. Blanc, and B. Dussardier, "Three-hole microstructured optical fiber for efficient fiber Bragg grating refractometer," Opt. Lett. **32**(16), 2390–2392 (2007).
32. A. Candiani, A. Bertucci, S. Giannetti, M. Konstantaki, A. Manicardi, S. Pissadakis, A. Cucinotta, R. Corradini, and S. Selleri, "Label-free DNA biosensor based on a peptide nucleic acid-functionalized microstructured optical fiber-Bragg grating," J. Biomed. Opt. **18**(5), 057004 (2013).
33. L. Rindorf, J. B. Jensen, M. Dufva, L. H. Pedersen, P. E. Høiby, and O. Bang, "Photonic crystal fiber long-period gratings for biochemical sensing," Opt. Express **14**(18), 8224–8231 (2006).
34. T. Wieduwilt, J. Dellith, F. Talkenberg, H. Bartelt, and M. A. Schmidt, "Reflectivity enhanced refractive index sensor based on a fiber-integrated Fabry-Perot microresonator," Opt. Express **22**(21), 25333–25346 (2014).
35. R. M. André, S. Pevec, M. Becker, J. Dellith, M. Rothhardt, M. B. Marques, D. Donlagic, H. Bartelt, and O. Frazão, "Focused ion beam post-processing of optical fiber Fabry-Perot cavities for sensing applications," Opt. Express **22**(11), 13102–13108 (2014).
36. W. Yuan, F. Wang, A. Savenko, D. H. Petersen, and O. Bang, "Note: optical fiber milled by focused ion beam and its application for Fabry-Pérot refractive index sensor," Rev. Sci. Instrum. **82**(7), 076103 (2011).
37. J. Feng, M. Ding, J.-L. Kou, F. Xu, and Y.-Q. Lu, "An optical fiber tip micrograting thermometer," IEEE Photonics J. **3**(5), 810–814 (2011).
38. K. P. Nayak, F. Le Kien, Y. Kawai, K. Hakuta, K. Nakajima, H. T. Miyazaki, and Y. Sugimoto, "Cavity formation on an optical nanofiber using focused ion beam milling technique," Opt. Express **19**(15), 14040–14050 (2011).
39. Y. Liu, C. Meng, A. P. Zhang, Y. Xiao, H. Yu, and L. Tong, "Compact microfiber Bragg gratings with high-index contrast," Opt. Lett. **36**(16), 3115–3117 (2011).
40. C. Martelli, P. Olivero, J. Canning, N. Groothoff, B. Gibson, and S. Huntington, "Micromachining structured optical fibers using focused ion beam milling," Opt. Lett. **32**(11), 1575–1577 (2007).
41. C. M. B. Cordeiro, C. J. S. de Matos, E. M. dos Santos, A. Bozolan, J. S. K. Ong, T. Facincani, G. Chesini, A. R. Vaz, and C. H. Brito Cruz, "Towards practical liquid and gas sensing with photonic crystal fibres: side access to the fibre microstructure and single-mode liquid-core fibre," Meas. Sci. Technol. **18**(10), 3075–3081 (2007).
42. F. Wang, W. Yuan, O. Hansen, and O. Bang, "Selective filling of photonic crystal fibers using focused ion beam milled microchannels," Opt. Express **19**(18), 17585–17590 (2011).

#250288 Received 16 Sep 2015; revised 15 Dec 2015; accepted 21 Dec 2015; published 7 Jan 2016

43. S. C. Warren-Smith, H. Ebendorff-Heidepriem, T. C. Foo, R. Moore, C. Davis, and T. M. Monro, "Exposed-core microstructured optical fibers for real-time fluorescence sensing," Opt. Express **17**(21), 18533–18542 (2009).
44. R. Kostecki, H. Ebendorff-Heidepriem, S. C. Warren-Smith, and T. M. Monro, "Predicting the drawing conditions for microstructured optical fiber fabrication," Opt. Mater. Express **4**(1), 29–40 (2014).
45. R. Kostecki, H. Ebendorff-Heidepriem, C. Davis, G. McAdam, S. C. Warren-Smith, and T. M. Monro, "Silica exposed-core microstructured optical fibers," Opt. Mater. Express **2**(11), 1538–1547 (2012).
46. F. M. Cox, R. Lwin, M. C. J. Large, and C. M. B. Cordeiro, "Opening up optical fibres," Opt. Express **15**(19), 11843–11848 (2007).
47. P. Toupin, L. Brilland, C. Boussard-Pledel, B. Bureau, D. Mechin, J.-L. Adam, and J. Troles, "Comparison between chalcogenide glass single index and microstructured exposed-core fibers for chemical sensing," J. Non-Cryst. Solids **377**, 217–219 (2013).
48. C. Perrella, H. P. Griesser, P. S. Light, R. Kostecki, T. M. Stace, H. Ebendorff-Heidepriem, T. M. Monro, A. G. White, and A. N. Luiten, "Demonstration of an exposed-core fiber platform for two-photon rubidium spectroscopy," Phys. Rev. Appl. **4**(1), 014013 (2015).
49. S. C. Warren-Smith and T. M. Monro, "Exposed core microstructured optical fiber Bragg gratings: refractive index sensing," Opt. Express **22**(2), 1480–1489 (2014).
50. S. C. Warren-Smith, R. Kostecki, L. V. Nguyen, and T. M. Monro, "Fabrication, splicing, Bragg grating writing, and polyelectrolyte functionalization of exposed-core microstructured optical fibers," Opt. Express **22**(24), 29493–29504 (2014).
51. C. A. Volkert and A. M. Minor, "Focused ion beam microscopy and micromachining," MRS Bull. **32**(05), 389–399 (2007).
52. Heraeus, "Quartz glass for optics - data and properties", retrieved 9 July 2015, http://heraeus-quarzglas.com/media/webmedia_local/downloads/broschren_mo/DataandProperties_Optics_fusedsilica.pdf.

1. Introduction

The concept of fabricating optical fibers using a structural combination of glass and air was first demonstrated by Kaiser *et al.* in 1974 [1]. This technique was seen as a method of producing low-loss fibers from a single material, while allowing the core to be protected from the external environment. Further development in the 1990s introduced microstructured holes into the optical fiber cross-section, giving rise to unprecedented control of the fiber's optical propagation properties [2, 3]. Various designs of microstructured optical fiber (MOF) have since proven useful for: endlessly single-mode guidance [4], air-core guiding [5], high non-linearity [6], supercontinuum generation [7, 8], and double-clad structures for fiber-lasers [9–11].

An area of particular interest is chemical and biological sensing, whereby the holes of a MOF can be filled with liquid or gaseous analytes that interact with the portion of the optical mode propagating within the fiber holes [12, 13]. This platform offers high sensitivity due to long interaction lengths, while requiring only small sample volumes [13, 14]. The cross-sectional structure of the MOF can be tailored to increase the measurement sensitivity, which involves increasing the interaction of the propagating mode(s) with the analyte to be sensed. This is achieved by reducing the core diameter of the fiber so that the evanescent field is substantial [15, 16] or by making use of liquid-core structures [17, 18].

Demonstrated sensing configurations and applications are diverse, including: hydrogen peroxide sensing using Raman scattering [19], fluorescent indicator coatings for detection of aluminum [20] and calcium and cadmium ions [21], absorption spectroscopy of biomolecules [22], and the use of fluorescent labeling techniques for antibodies [23] and proteins [24]. There are also numerous examples of microstructured optical fiber sensing techniques that measure changes in the refractive index of the material filled into the fiber holes [14], such as: techniques based on multimode interferometry [25], multi-core mode-coupling [26], and surface plasmon resonance [27–30].

New fabrication and processing techniques allow expansion upon the cross sectional design of a MOF by adding structure along the fiber core. For example, fiber Bragg gratings [31, 32] and long period gratings [33] have been written for sensing applications. To expand the scope of structures that can be fabricated, focused ion beam (FIB) milling is an ideal platform that has been proven for fabricating high resolution features in micro-fibers such as Fabry-Perot cavities [34–36] and fiber Bragg gratings [37–39]. However, the application of

#250288 Received 16 Sep 2015; revised 15 Dec 2015; accepted 21 Dec 2015; published 7 Jan 2016

such techniques to MOFs is challenging because the core is protected by the outer cladding. To date, the use of focused-ion beam milling with MOFs has been limited to opening side holes through the cladding of MOFs [40, 41] or writing channels on the end face of the MOF, forming micro fluidic channels when the fiber is spliced [42].

In this paper, we demonstrate the fabrication of optical features directly onto the core of a MOF using focused ion beam milling. To gain access to the fiber's core, we used a unique MOF, exposed-core microstructured optical fiber (ECF), where a portion of the external cladding has been removed in the fabrication process [43–48]. Longitudinal structuring of ECFs has recently been demonstrated via femtosecond laser ablation Bragg gratings [49, 50]. Here we expand the tool-kit for structuring ECFs by demonstrating the inscription of two different designs of Fabry-Perot cavity directly onto the core using focused-ion beam milling. The first cavity cuts through the ECF core, penetrating into the internal holes of the fiber and forming reflecting surfaces across the entire core. The second cavity is a shallow rectangle milled into the center of the core such that it does not penetrate into the internal ECF holes. These two cavity designs were chosen to demonstrate the versatility of the technique. We envision that when applied to sensing, the penetrating cavity can be of use for gas sensing or in a microfluidic configuration with fluid pumped through the far end of the fiber while the shallow cavity can be optimized to be particularly sensitive to surface interactions for biological sensing.

2. Fiber geometry and splicing

The exposed-core microstructured optical fiber (ECF) used here was fabricated using the same technique as previously reported [44, 45, 50]. The preform was fabricated from a 20 mm outer diameter, 100 mm long fused silica glass rod (Suprasil F300, Heraeus). Three holes were ultrasonically drilled into the center of the rod in an equilateral triangle configuration with 0.4 mm hole separation. A 1 mm slot was cut into one of the holes using a diamond blade, exposing the core. The preform was drawn with a furnace temperature of 2010°C and positive internal hole pressure (the two closed holes) of 11 mbar. The resulting fiber, shown in Fig. 1, has an outer diameter of 160 μm and an effective core diameter of 6.8 μm, where the effective core diameter is defined as the radius of a circle whose area is the same as a triangle that fits wholly within the core.

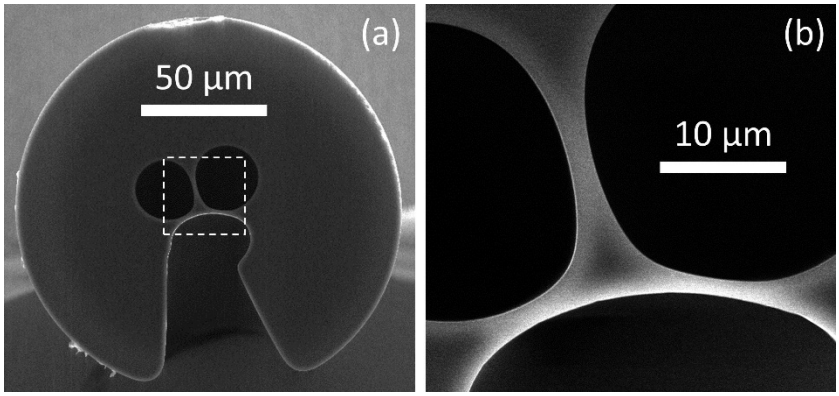

Fig. 1. Scanning electron microscope (SEM) images of the entire microstructured exposed-core fiber (ECF) cross-sectional geometry (a) and of the core region (b).

Two separate ECFs, with lengths of approximately 30 mm, were spliced to conventional single mode fibers (SMF28e) using a previously optimized technique for a similar structure [50]. In this technique, a conventional arc splicer (Fujikura FSM-100P) set for a standard SMF28-SMF28 splice was used, however the arc current was reduced by 4.0 mA and arc time increased to 3.0 s. Manual alignment was used and assessed via transmitted power measured

#250288 Received 16 Sep 2015; revised 15 Dec 2015; accepted 21 Dec 2015; published 7 Jan 2016

on a power meter. Images of a typical splice are shown in Figs. 2(a) and 2(b). Note that the far end of the ECF was sealed (melted) using the arc splicer, which has been found to be effective in removing reflections from the far end of the fiber.

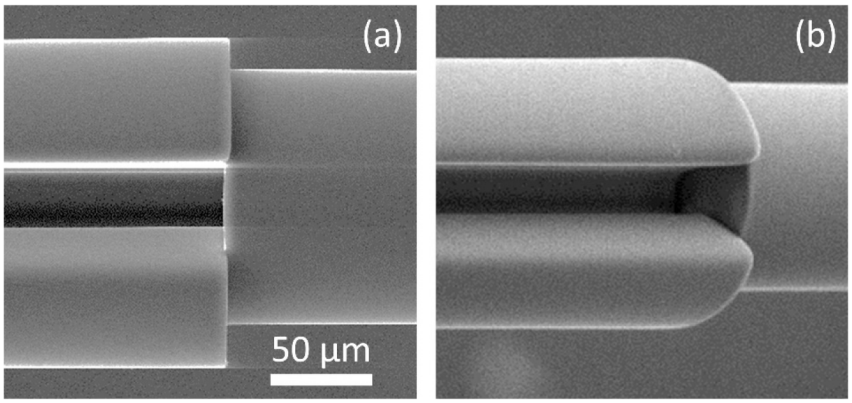

Fig. 2. Scanning electron microscope (SEM) image of the splice between the ECF and a conventional single mode fiber (SMF28e). (a) Viewed perpendicularly to the optical axis, directly into the cladding opening. (b) Viewed at a 45° angle. For reference, the diameter of the ECF (left) is 160 µm while the SMF28e (right) is 125 µm.

3. Focused ion beam milling

3.1 Sample preparation

To demonstrate that structure can be written directly onto the core of an exposed-core fiber, two different Fabry-Perot cavities were written using a Tescan (Lyra XMU) FIB-SEM (focused ion beam – scanning electron microscope). First, the two spliced fibers were mounted onto an aluminum block using a silver paste. A microscope was used to rotate the fiber such that the open section of the ECF was vertically orientated prior to gluing. The sample was then sputter coated with a 50 nm tantalum coating to reduce charging effects in the electron/ion microscope.

3.2 Structure 1: Penetrating cavity

The first cavity, which penetrated into the internal ECF holes, required four machining steps; SEM images of the first three steps are shown in Figs. 3(a)-3(c). (1) A large square milling pattern was used to open the ECF internal holes and partially remove the core using a high beam current (I ≈2 nA) for a duration of 75 min [Fig. 3(a)]. This opening exposed the position of the core, but did not form an optical cavity due to a curved surface finish. (2) A polishing step formed two parallel reflecting surfaces on the core using a lower current (I ≈600 pA) for a duration of 55 min [Fig. 3(b)]. (3) The remaining central core structure was removed using a smaller milling rectangle than in step 1 (I ≈600 pA, duration = 45 min), see Fig. 3(c). (4) Finally, the 50 nm tantalum coating was removed along the core between the splice point and the cavity using a 35 µm width rectangular pattern centered on the core and a high beam current (I ≈2 nA). The tantalum coating leads to significant optical loss (discussed in Sec. 4) and FIB milling is an effective and clean means of removing the coating. A thin layer, less than 150 nm, of the ECF may have been removed during this step, however this is negligible compared to the core diameter (6.8 µm). The final cavity had a length of 34.6 µm [Fig. 3(d)] and the splice was 434 µm from the start of the cavity [Fig. 3(e)].

#250288 Received 16 Sep 2015; revised 15 Dec 2015; accepted 21 Dec 2015; published 7 Jan 2016

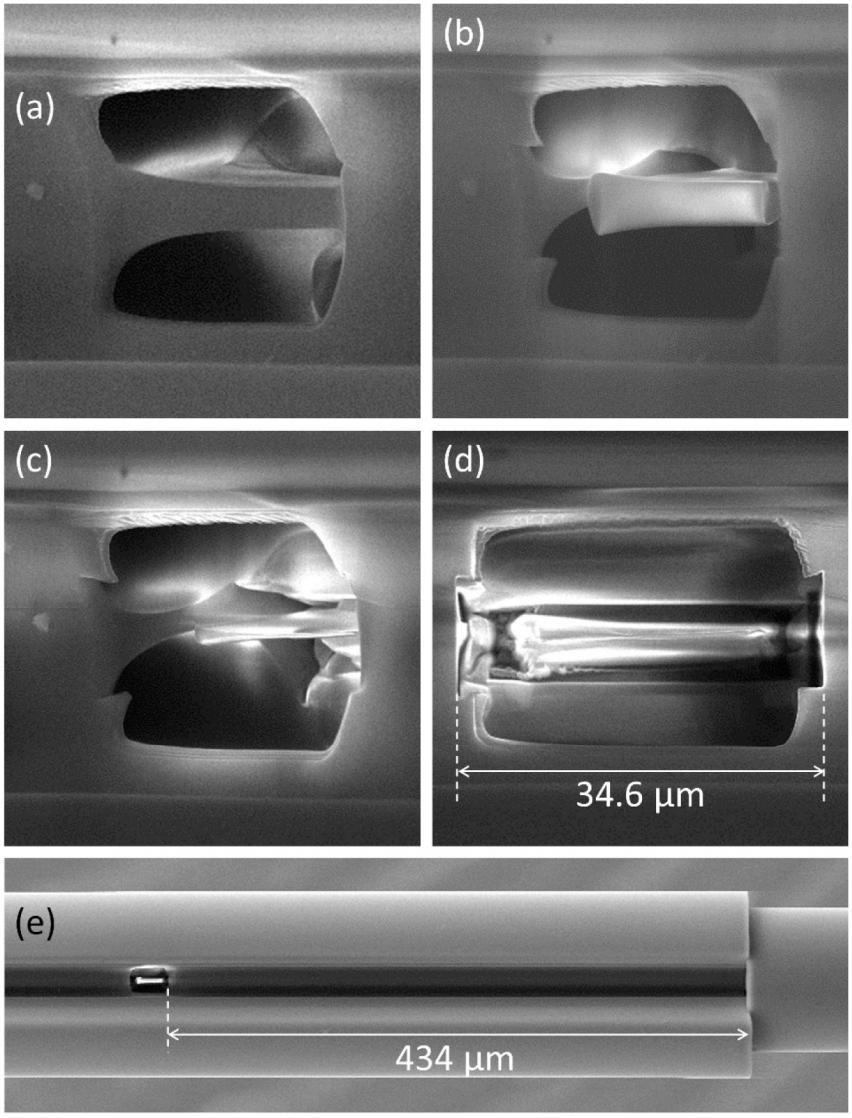

Fig. 3. The procedure used for fabricating Fabry-Perot cavities that cut through the entire core of the ECF, viewing down into the slot of the ECF. Images (a)-(c) were taken with a 45° viewing angle while (d) and (e) were taken perpendicularly to the fiber core. (a) A square milling pattern was used first to open the geometry with high current (I ≈2 nA). (b) The two end faces were polished with lower current (I ≈600 pA). (c) The remaining central material was removed. (d) The final Fabry-Perot cavity was measured to be 34.6 µm long. (e) The length of the ECF from the splice to the cavity was measured to be 434 µm.

3.3 Structure 2: Shallow (non-penetrating) cavity

The second cavity fabricated was a shallow cavity that did not penetrate into the holes of the ECF, shown in Fig. 4. The transverse positioning of the cavity was achieved though comparison to SEM images of the fiber's cross section [Fig. 1]. Control of the depth of the cavity was based on the FIB milling instrumental pre-calibrated values (milling time = 12 minutes for I ≈630 pA). The intended depth was 4.0 µm; however, the achieved milling depth is highly dependent on the ion beam incident angle [51]. The milling rate is generally greater at higher incident angles, peaking at approximately 75°, while normal incidence milling

#250288 Received 16 Sep 2015; revised 15 Dec 2015; accepted 21 Dec 2015; published 7 Jan 2016

occurs at a relatively slower rate. The final cavity depth was 2.0 μm, which was measured by viewing the cavity at 45°, as seen in Fig. 4(b).

As with the first cavity, the ends of the cavity were polished in order to produce optically flat surfaces with minimal off-axis angle. In contrast to the fully penetrating cavity, polishing must be performed with care to ensure there is no intrusion into the holes of the ECF. The polishing was thus performed in multiple small steps with increasing depth to take into account the slightly sloped surface of the cavity. The final step was to remove the tantalum coating, with the same procedure as the first cavity. The resulting cavity had a length of 28.9 μm [Fig. 4(a)], a width of 2.5 μm [Fig. 4(b)], and the distance from the splice to the start of the cavity was 524 μm [Fig. 4(c)].

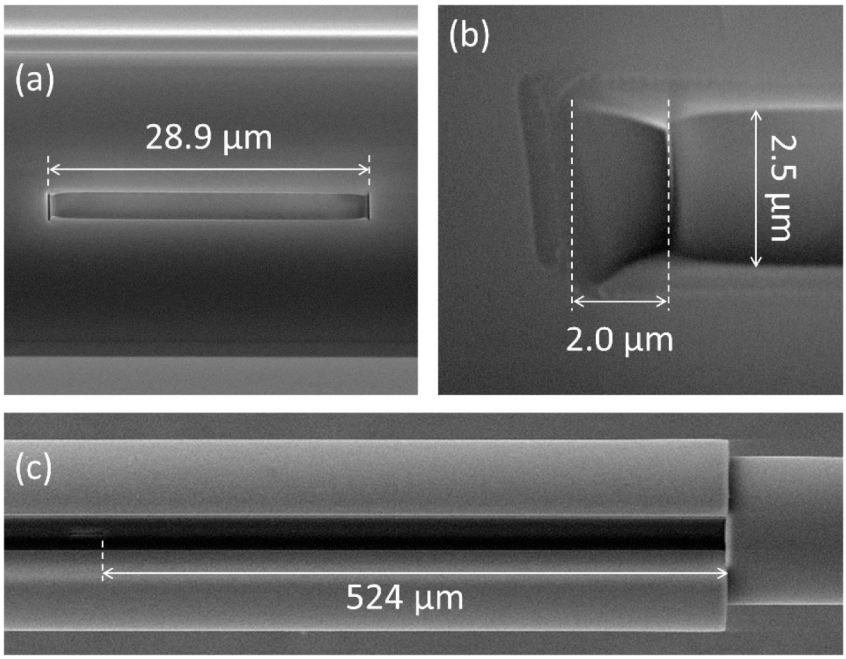

Fig. 4. (a) The shallow Fabry-Perot cavity in the core of the ECF. The upper and lower horizontal lines are a result of the walls of the open wedge structure of the ECF (see Fig. 1). (b) The left hand side cavity wall in (a), but viewed at an angle of 45° in order to measure the cavity depth. The measurement of 2.0 μm was after multiplying by √2 to take into account the viewing angle. (c) The length of the ECF from the splice to the cavity was measured to be 524 μm.

4. Optical characterization

The reflection spectra of the two different cavities, before and after the tantalum coating was removed, were characterized using a super-continuum source (Fianium, WL-SC-400-2), a circulator with FC/APC connectors, and an optical spectrum analyzer (ANDO, AQ6315). The measured wavelength range was 1200 nm to 1700 nm, performed in 50 nm steps with a resolution of 0.1 nm and later combined. This ensured sufficient resolution for measurement of the short free spectral range associated with the cavity formed by the splice and the FIB milled cavity. To obtain a reflectivity spectrum, the source spectrum, the circulator response, and OSA sensitivity were calibrated and removed from the cavity reflectivity spectra by measuring and normalizing to the reflectivity of a flat-cleaved SMF (that is, without the ECF present). The reflectivity of the flat-cleaved SMF is analytically well known and was calculated using the Sellmeier equation for F300 silica glass [52] and the normal incidence Fresnel reflection equation (e.g. 3.35% at 1200 nm and 3.28% at 1700 nm).

#250288 Received 16 Sep 2015; revised 15 Dec 2015; accepted 21 Dec 2015; published 7 Jan 2016

Subsequent Fourier transform analysis required conversion of the optical spectrum analyzer data to the frequency domain, as the free spectral range expressed in terms of wavelength is non-uniform [FSR_λ, Eq. (1)], while it is uniform when expressed in terms of optical frequency [FSR_ν, Eq. (2)].

$$FSR_\lambda = \Delta\lambda = \frac{\lambda^2}{2nl} = \frac{\lambda^2}{OPD}, \tag{1}$$

$$FSR_\nu = \Delta\nu = \frac{c}{2nl} = \frac{c}{OPD}, \tag{2}$$

where λ is the free space wavelength, c is the speed of light constant, n is the refractive index of the cavity, l is the cavity length, and OPD is the optical path difference between the two reflecting interfaces. The resulting reflection spectra, expressed in optical frequency, are shown in Figs. 5(a) and 5(b) for the penetrating and the shallow cavities, respectively. A subset of the full measured spectrum is shown, corresponding to a wavelength range from 1200 nm to 1300 nm, in order to display the narrow fringes associated with the cavity formed between the splice and cavity.

Two dominant fringes are present in the reflection spectra. For the first cavity [Fig. 5(a)], a fringe is present with a relatively large free spectral range (4.7 THz) corresponding to the milled cavity, and another with a smaller free spectral range (0.24 THz) corresponding to the cavity formed between the splice and the FIB milled cavity. There was no measured reflection from the far end of the ECF as the 30 mm long tantalum coating beyond the cavity strongly attenuated the optical signal, which also prevented transmission measurements. In addition, to ensure the far end did not contribute ambiguous signals to the reflected measurements it was sealed (melted) using an arc splicer. While the reflection from the splice might be considered a hindrance in this measurement, it is possible to de-multiplex the different cavities making it possible to simultaneously measure another physical parameter such as temperature or strain. De-multiplexing using fast Fourier transform techniques is discussed below.

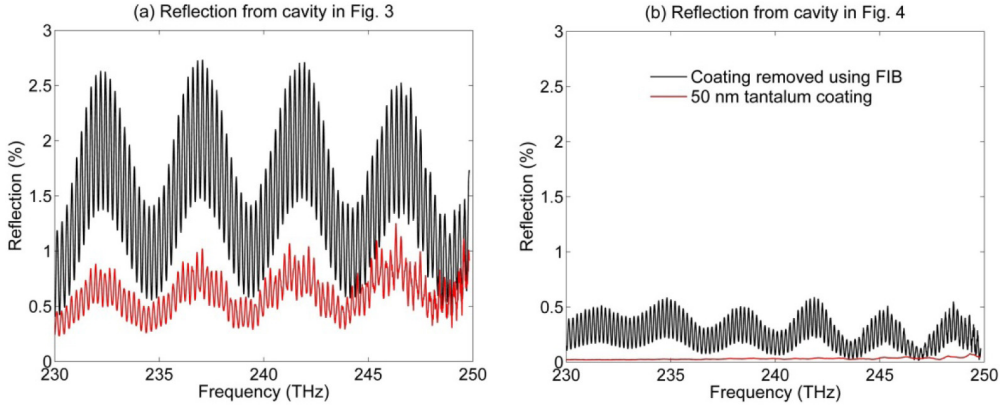

Fig. 5. Reflection of the Fabry-Perot cavity shown in (a) Fig. 3 and (b) Fig. 4. The reflectivity was normalized to the reflection of a cleaved single-mode fiber. That is, approximately 3.3% on the graph (just above the top) corresponds to reflection from a single glass-air interface. The reflection is shown for the case where the 50 nm tantalum coating is present (red) and after it was removed using the focused ion beam (black).

The peak reflectivity for the shallow cavity [Fig. 5(b)] is weaker by a factor of approximately five compared to the first cavity, due to a smaller overlap factor with the propagating optical modes. This is not surprising given the cavity depth is 2.0 μm compared to a core diameter of 6.8 μm. The shallow cavity differs significantly before and after the

#250288 Received 16 Sep 2015; revised 15 Dec 2015; accepted 21 Dec 2015; published 7 Jan 2016

tantalum coating was removed, the red and black curves respectively in Fig. 5(b). Given the cavity does not penetrate deeply into the core, propagating higher order modes with greater energy at the surface, predominantly contribute to the reflectivity seen in Fig. 5(b) while also experiencing greater loss when a metal coating is present. Thus, the removal of metal coatings is particularly important if considering surface-based structures using focused ion beam milling techniques and use of FIB milling to remove the coating is a viable option.

The reflectivity at each interface is relatively weak, limited to ≤3.35%, as they are generated from either a full or partial glass-air interface respectively for the penetrating cavity and the shallow cavity, as well as the SMF-ECF splices. Thus, multiple reflections can be considered negligible and the cavity considered to be a two-wave interferometer with a sinusoidal dependence. Performing a fast Fourier transform (FFT) on the reflection spectra thus leads to a single peak for each pair of reflections: (1) reflection from the two cavity walls (2) reflection at the splice and the first cavity wall (M1), and (3) reflection at the splice and the second cavity wall (M2). To this effect, the FFT of the reflected spectra of the two cavities was performed and is shown in Fig. 6.

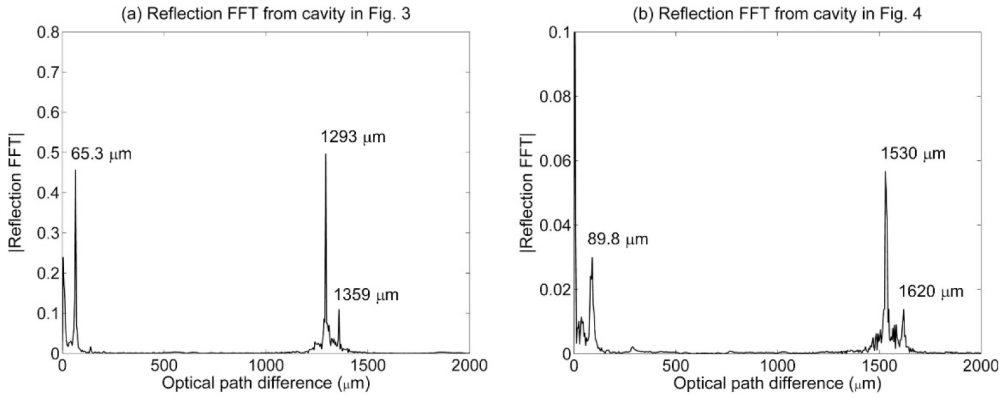

Fig. 6. Fast Fourier transform (FFT) of the spectra measured from the cavities in (a) Fig. 3 and (b) Fig. 4. The x-axis is displayed as optical path difference (OPD) using Eq. (2).

Table 1. Cavity Length: Comparison of Optical Measurements with SEM Measurements[a]

Cavity	Reflection interfaces	l_{air} (μm)[b]	l_{glass} (μm)[c]	l_{SEM} (μm)
Penetrating	M1 and M2	**32.7**	22.6	**34.6**
(Fig. 3)	Splice and M1	647	**448**	**434**
	Splice and M2	680	471	469
Shallow	M1 and M2	44.9	**31.1**	**28.9**
(Fig. 4)	Splice and M1	765	**529**	**524**
	Splice and M2	810	**560**	**553**

[a] Values that are expected to match well are indicated in bold.
[b] Measurements from Fig. 6, with values divided by *2n* to give cavity length assuming n = 1.000.
[c] Measurements from Fig. 6, with values divided by *2n* to give cavity length assuming n = 1.445 (the mean refractive index of F300 silica glass over the range λ = 1200 nm to λ = 1700 nm).

The position of the three main peaks can be used to measure the optical path difference of each reflecting pair, achieved by converting the x-axis of the FFT using Eq. (2). Table 1 presents each peak position, where the optical path difference has been divided by *2n* in order to represent the cavity length for the cases of air (n = 1.000) or silica glass (n = 1.445). It can be seen that for both of the fabricated cavities the cavity length associated with the splice and the first reflecting surface (M1) matches the SEM measurement when the glass refractive index is used. This is expected as the fundamental mode of the ECF should have an effective index close to the refractive index of glass given the fiber is relatively multimode with a large numerical aperture. When considering the milled cavity (reflections at M1 and M2), the

#250288 Received 16 Sep 2015; revised 15 Dec 2015; accepted 21 Dec 2015; published 7 Jan 2016

penetrating cavity measurements agree well when the cavity index is assumed to be that of air. In contrast, the shallow cavity is found to have a refractive index of glass, indicating that the modes associated with this cavity are still predominantly guided within the glass core of the fiber.

The close agreement between the SEM measured and the optical reflection measured values demonstrate that we have indeed milled optically functioning structures into the core of the exposed-core microstructured optical fiber. These results also demonstrate that the different cavities can be readily de-multiplexed, allowing for simultaneous measurement of different parameters (e.g. refractive index, temperature, and strain). In principle, additional cavities could be written along a single ECF to increase the number of parameters that can be measured. This can be with great flexibility in spatial separation given the low loss guidance of the ECF (e.g. relative to a taper), provided the metal coating can be appropriately deposited and/or removed.

5. Conclusions

We have employed focused ion beam milling to fabricate optical structures directly onto the core of a microstructured optical fiber. In order to gain access to the core we have used an exposed-core microstructured optical fiber, which has a portion of the cladding removed during the fabrication process. We have written two different types of Fabry-Perot cavities, which serve effectively as two-wave interferometers. The versatility and resolution of focused ion beam milling allows for control of the type of cavity, and here we utilize this to demonstrate both a cavity that cuts entirely across the fiber core into the holes of the MOF and a shallow cavity on the surface of the MOF core. Both cavities were characterized optically and the resulting interference spectra match well with the SEM measured cavity lengths, thus confirming their optical function. We have also demonstrated that focused ion beam milling can be used for removing the metal coating, which was initially deposited to reduce charging effects in the FIB/SEM microscope.

While focused ion beam systems are a mature commercial technology, they are expensive instruments and milling times can be considerable. The total milling times used in our experiments were approximately three hours for the larger (penetrating) cavity and 12 minutes for the smaller (non-penetrating) cavity. Thus, we anticipate our technique will be of use primarily for prototyping, or producing specialized devices that specifically require precise micro/nano-structuring along the optical axis in combination with control of the cross sectional geometry (e.g. dispersion) and standard fiber connectorization.

Acknowledgments

Stephen Warren-Smith is funded by the European Commission through the Seventh Framework Programme (FP7), PIIF-GA-2013-623248. Ricardo André is funded by Fundação para a Ciência e Tecnologia through the grant SFRH/BD/84048/2012. The authors would like to acknowledge the ARC Centre of Excellence for Nanoscale Biophotonics (CE14010003) for providing the exposed core fiber. This work was performed in part at the OptoFab node of the Australian National Fabrication Facility utilizing Commonwealth and South Australian State Government funding.

#250288 Received 16 Sep 2015; revised 15 Dec 2015; accepted 21 Dec 2015; published 7 Jan 2016